Accepted Manuscript

High-resolution computed tomography in resin infused woven carbon fibre composites with voids

S.M. Sisodia, S.C. Garcea, A.R. George, D.T. Fullwood, S.M. Spearing, E.K. Gamstedt

PII: S0266-3538(16)30354-2

DOI: 10.1016/j.compscitech.2016.05.010

Reference: CSTE 6425

To appear in: *Composites Science and Technology*

Received Date: 12 January 2016

Revised Date: 5 May 2016

Accepted Date: 20 May 2016

Please cite this article as: Sisodia SM, Garcea SC, George AR, Fullwood DT, Spearing SM, Gamstedt EK, High-resolution computed tomography in resin infused woven carbon fibre composites with voids, *Composites Science and Technology* (2016), doi: 10.1016/j.compscitech.2016.05.010.

Significance of paper

Recent efforts in the composites industry towards less-expensive means to produce high-performance parts have often involved optimisation of liquid composite moulding processes such as resin transfer moulding (RTM). The most significant gap in part quality between RTM manufactured parts and traditional autoclave processes is the usually higher void content in the former, arising from the entrapment of bubbles during infusion, and the lower consolidation pressures used during such processes. Many laboratories around the world are working on understanding bubble entrapment and subsequent bubble mobility, so as to optimise RTM processes to reduce the concentration and size of voids. This paper contributes to that understanding with three-dimensional examination using CT imaging of the morphology, size, clustering and location of the individual voids in composite parts made with RTM.

Most important / novel contributions

This paper presents visualisation of the voids in a composite part with significantly more statistical information regarding size distribution, orientation and location than has been previously shown in the literature. It also addresses a reinforcement architecture more typical to RTM, an un-balanced weave, than the unidirectional fabrics usually studied in previous work on void formation. Analysing a complex reinforcement along with the enhanced visualisation abilities of the CT-imaging technique allowed novel observations and conclusions regarding voids:

1) As the orientation angle between a reinforcement layer and the resin flow direction increases from parallel to perpendicular, larger voids and a greater number of voids were observed in that layer. This was linked to the resulting greater propensity for fatigue crack propagation between voids in layers transverse to the loading direction. A simple optimisation strategy is thus to infuse in a direction transverse to the expected primary load direction, thus creating the fewest voids in the transverse-to-load direction.
2) Voids accumulate around both the layer interfaces and yarns and are nearly completely absent from the layer thickness between those interfaces and away from yarns.
3) Void distribution follows the orientation of fibres in adjacent layers, suggesting that out-of-plane flow is a significant mechanism in void formation and mobility.
4) Observations 1-3 above all imply that current void formation and mobility models must be expanded from a microscale approach to the laminate scale, in order to focus on out-of-plane bubble movement and yarn bubble entrapment.

High-resolution computed tomography in resin infused woven carbon fibre composites with voids

S.M. Sisodia[1,2], S.C. Garcea[3], A.R. George[4], D.T. Fullwood[4], S.M. Spearing[3], and E.K. Gamstedt[1*]

[1]Uppsala University, Department of Engineering Sciences, Division of Applied Mechanics, SE-75121 Uppsala, Sweden

[2]GKN Aerospace, Redditch, Worcestershire, United Kingdom

[3]Materials Research Group, Faculty of Engineering and the Environment, University of Southampton, Southampton, United Kingdom

[4]Manufacturing Engineering Technology, Brigham Young University, Provo, UT 84602, USA

Abstract

Tomographic imaging using both microfocus radiation and synchrotron radiation was performed to assess the void defects in resin transfer moulded woven carbon fibre composites. The focus of this study is on characterising the void homology (e.g. local void size and spatial distribution) in relation to weave orientation, infusion direction and potential effects on damage formation in tensile loading. As the orientation angle between the fibre direction of unidirectional layer in the laminate and the direction of the global resin flow increases, from parallel to perpendicular, larger voids and a greater volume fraction of voids were observed, which led to increased damage formation upon loading. Significant accumulation of voids around both the layer interfaces and yarn fibres were also observed. With regard to yarn design, it is recommended to balance the benefits (e.g. fabric handling, structural integrity of preform) and drawbacks (e.g. lower fibre content, more voids) of the supporting yarn. Also, sensible placement of resin inlets and outlets could reduce the amount of deleterious voids, i.e. by promoting resin flow along the fibre direction in the most defect-sensitive off-axis layers.

Keywords: (A) Textile composites, (B) Defects, (B) Porosity/Voids, (E) Resin transfer moulding (RTM), (unlisted) X-ray computed tomography (CT).

1. Introduction

The composites industry has traditionally made high performance primary structural components out of pre-impregnated reinforcements cured in an autoclave oven. The high pressures involved in such processes and the unidirectional fibres in the constituent layers result in high fibre content and minimal void formation. Non-autoclave composite manufacturing processes such as resin transfer moulding (RTM) have lower cycle times, reduced operating costs and require less capital investment. However, RTM results in more voids in the laminate due to entrapment of air bubbles during filling [1,2]. Voids are known to be detrimental to the mechanical performance of the material [3-10]. A deeper understanding of the formation of voids, and their effect on damage and mechanical performance is desirable in the context of improving the performance of RTM and other non-autoclave manufactured components.

The practical importance of voids has prompted research into the mechanisms behind void formation in RTM (see e.g. the review article by Park and Woo [2]). The study of the mechanical entrapment of voids in composites consisting of fibre bundles, such as woven fabrics, usually relates to the formation of intrabundle micro-voids and

* Corresponding author. Tel.: +46 704-250-382
E-mail address: kristofer.gamstedt@angstrom.uu.se (Kristofer Gamstedt)

interbundle macro-voids due to the relative flow velocities of the infusion resin inside and outside the fibre bundles [11]. Higher applied pressures result in faster macro-flow in between the fibre bundles, outpacing the capillary wicking flow into the tightly packed fibre bundles, thus creating entrapment of intrabundle bubbles [12]. The majority of these bubbles remain trapped at the location of formation due to the densely packed fibre architecture [13,14] and eventually diffuse into solution (i.e. Henry's law) as the local pressure rises with the advancing flow [15]. The opposite case occurs with a low applied pressure. As the fluid flow velocity is decreased, the macroscale interbundle primary flow is outpaced eventually by the intrabundle capillary flows. The secondary intrabundle flow seeps into the interbundle gaps at various places ahead of the macro interbundle flow front, thus entrapping relatively large interbundle bubbles [1,16]. These interbundle bubbles often escape the laminate by travelling quickly between the bundles to the flow front and bursting into the vacuum at the vent [17]. The chance of these larger bubbles escaping depends on the interbundle gap width, the applied pressure, and the bubble size. As the resin pressure increases with the advancing flow front, the driving pressure behind the bubbles increases, and the size of the bubbles decreases according to both the Ideal Gas Law and Henry's Law until a critical bubble size is reached, allowing escape [15,18,19].

Current attempts are being made to couple void formation and void movement models to be able to predict the final distribution [20,21]. These models would assist in RTM process optimisation for high-performance composites, however, they are limited by (i) the difficulty of measuring *in situ* void formation [22,23], and (ii) the complexity of fluid dynamics modelling for the various flow paths and fibre architectures in industrial RTM processes. Recent work has analysed in-plane flow through fibre bundles arranged at 45° and 90° with respect to the flow [20], and experimental void formation has been reported for biaxial weaves [16,24], although the majority of the relevant literature has considered only unidirectional (UD) fibres parallel to the flow direction. The present study undertakes experimental void characterisation to assist in understanding the flow paths and subsequent void formation in a more complex fabric; a quasi-isotropic layup woven plies.

Previous work has investigated the influence of voids on mechanical properties [3-10], most having focused on prepreg materials. As the microstructure and constituents in composites manufactured with resin infusion processes are usually different from those in autoclave-cured prepregs, the effects of defects on mechanical properties must still be established in RTM composites to pave the way for determining design allowables for the void contents.

Failure mechanisms associated with voids in loading modes such as transverse tensile [8] and multi-axial fatigue, both flexural [4] and in tension [9], have been investigated. The aim of understanding such mechanisms is to allow strategies to suppress damage growth and increase the mechanical performance. Potentially, mechanism-based models could be used to decrease the amount of required testing. Such simulation tools will require an understanding of the effects of void size, shape, location, clustering, and concentration [10,25]. Traditional approaches to quantifying voids are typically limited to the average void volume fraction throughout the entire part. This is a single parameter, which is of limited use in determining local microstructural effects. Unlike prepreg processing [3-7], void concentrations are not

homogeneous in resin infusion processes such as RTM due to the pressure gradient resulting from infusion and the often more heterogeneous microstructure of the fibre preforms. The voids are also not homogeneous in size and shape due to the variety of bubble entrapment mechanisms governing void formation [11]. These complications for RTM composites imply a need for characterising the voids at a local level, i.e. allowing for spatial variation.

Conventional measurement techniques are not well-suited for local void characterisation in the composite microstructure. Optical microscopy and combustion/digestion only allow sampling of the voids in small volumes of the part [26]. Optical microscopy is also limited to two-dimensional (2-D) planar imaging, which can result in misleading interpretations of void shape, e.g. categorising long cylindrical voids as small ellipses from their cross-sections [11,13]. Combustion or digestion gives only the scalar void fraction, and no information regarding the void size, shape or clustering. Through-thickness optical measurement only works for transparent materials such as composites with glass fibre reinforcement [27]. Ultrasonic C-scan imaging is commonly used for quality control by detecting delamination and large dry spots. It has also been applied to detect general attenuation, which is in turn correlated to the void content, thus providing an estimate of local void concentrations across the entire part surface [4,28]. However, the ultrasonic wave-lengths are too large to provide sufficient resolution to determine void size and shape, and may not detect intrabundle micro voids at all [29].

X-ray computed tomography (CT) provides higher resolution than ultrasound, due to higher frequency and the fact that transmission imaging detects density variations whereas reflection imaging (ultrasound) only detects interfaces. Imaging by CT also results in reduced dispersion compared to ultrasound due to using electromagnetic radiation instead of sound waves. A three-dimensional (3-D) volume representational image can be constructed from the multiple projected images taken during sample rotation under the X-ray beam. CT imaging of composites has mostly been focused on prepreg materials [30-33]. In prepreg consolidation experiments, long thin cylindrical voids, which are parallel to the fibres have been discovered, showing the improved visualisation abilities compared to 2-D through-thickness microscopy which would show any such void as a pinhole [31,32]. CT imaging showed similar long thin voids in material prepared from compression-moulded prepregs [34]. The enhanced ability of 3-D volume rendering in CT imaging, to characterise void morphology, compared with 2-D microscopy has been illustrated [33]. Unprecedented quantifications of the distribution and size of individual voids have been achieved with CT imaging [33,34]. However, CT-imaging has not been widely used thus far for the void characterisation of resin-infused composite parts, with the exception of the study by Schell et al. [35] that presents 2-D scans of infusion-induced voids, and Vila et al. [23] that illustrates *in-situ* voids imaged during the process of infusion in a single fibreglass roving. The greater variation in local void size, shape and clustering makes CT-enabled 3-D visualisation of voids even more important in the case of infusion compared to laminated material produced from prepreg. In addition the use of synchrotron radiation computed tomography (SRCT) allows for higher resolution compared to lab-scale micro-focus CT (μCT).

The major limitations on CT-imaging are the cost of the equipment and the time required for data management to prepare and analyse the images. As equipment is improving and more efficient and user-friendly image analysis software is developed, CT is emerging as the preferred technique to characterise small-scale defects in composite materials. This study concerns a 3-D examination of the morphology, size, distribution, concentration and location (or homology) of the voids in composite samples made with RTM using X-ray CT, image analysis and statistical analysis. The intention of this study is to improve the understanding of the mechanisms of void formation during resin infusion into a complex multi-axial reinforcement preform and to detect defects that could affect in-service damage development.

2. Materials and methods

2.1. Laminate manufacture

Rectangular laminated composite plates of 800 mm × 400 mm × 4 mm were manufactured by RTM with unidirectional flow along the length using a constant pressure difference of 200 kPa. Hexcel's resin system HexFlow RTM 6 was used with an aerospace-grade unidirectional (UD) carbon fibre weave. The fabric architecture, shown in Fig. 1, consists of UD carbon fibre tows held together by biaxial woven glass fibre yarns in both warp and weft directions. The laminates were laid up with a quasi-isotropic stacking sequence of $[0/–45/90/+45]_{2s}$. The primary flow direction during infusion was along the 0° axis. Analysis of the CT images showed that the average fibre volume content was established to be 53%, with the carbon fibres comprising approximately 93% of the fibre volume. The areal total weight for the carbon fibre was 242.5 g/m^2 and glass fibre 13.5 g/m^2.

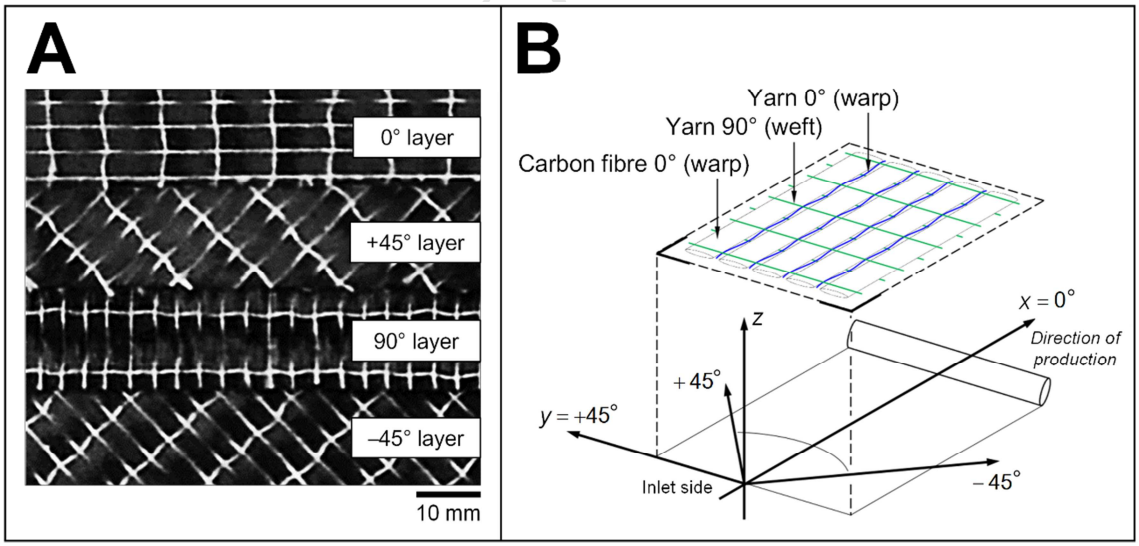

Fig. 1. (a) Photograph of fabric layers with different fibre orientations viewed from top, and (b) coordinate system for mould, fabric and laminate.

2.2. Imaging by X-ray computed tomography

3-D imaging using CT was performed on two different scales with complementary equipment: (i) using the Nikon Metrology HMX 225^{TM} µCT at the µ-VIS Centre at the

University of Southampton for wider fields of view, and (ii) using SRCT at the TOMCAT/X02DA beamline, at the Swiss Light Source of the Paul Scherrer Institut for high resolution imaging. Wide-field CT is suitable for capturing the larger interbundle and interlaminar voids in volumes representative of the overall layered structure, whereas SRCT is more suitable for microscale characterisation of smaller intrabundle voids.

The scan settings for both the µCT and the SRCT are given in Table 1. For SRCT, the sample was mounted vertically and orthogonal to the beam, with a propagation distance of 20 mm, allowing a degree of phase contrast to be achieved. The projections were collected through a rotation of 180˚ and 3-D reconstruction was achieved from the concatenated radiographs using an in-house code based on the GRIDREC/FFT approach [36]. Image analysis was performed using VG studio Max v2.1^{TM} and Avizo Fire 8^{TM}. In particular, voids were segmented in VG studio Max v2.1^{TM} using the seed-growing algorithm, then binarised and quantified using Avizo Fire 8^{TM}. The minimum feature size of void considered in the 2-D slices for both SRCT and µCT was 5 µm and 50 µm, respectively.

Parameter	**SRCT**	**µCT**
Sample size (mm^3)	30 × 4 × 4	
Acceleration voltage (kV)	Not applicable	60
Beam energy (keV)	14	Not applicable
Beam current (µA)	Not applicable	134
Voxel size (µm)	0.65	4.18
Detector dimensions (pixels)	2560 × 2160	2048 × 2048
Number of radiographs	1601	3142
Exposure time (ms)	90	500
Scan time (minutes)	15	270

Table 1. Scan settings for X-ray CT.

2.3. Two-point statistical analysis

The 3-D images of the specimens provide almost unprecedented details regarding void and fibre positioning, however in order to achieve the goals of this work a statistical measure (beyond that of simple volume fractions) is desirable. 3-D CT images of material microstructures contain an abundance of data, requiring large memory storage capabilities; a single image file requires approximately 4 megabytes. The main challenge in microstructural analysis lies in data reduction and processing of the information-rich 3-D images. The first and most common step is to use image processing to generate a digital representation of the 3-D microstructure, although in isolation this approach does not provide any information on the statistics of the microstructural features. A statistical two-point correlation method can be used, however, to provide such information from the 3-D volume; discussions of the method and its relevant advantages can be found in references [37,38]. This method can be used to quantify the effect of microstructure on manufacturing-induced defects by capturing the geometrical relationships between a given phase (such as glass) and induced voids, for example.

Based on a histogram of grayscale values, the 3-D image from the μCT scans is segmented into the three phases. The two-point autocorrelations of the void phase, for example, then indicate the probability that a given vector, which is randomly placed in the sample, will land with both its head and tail in the void phase. Since a very short vector is likely to remain entirely within a single void, a contour map of the correlations close to the origin represents the average shape of voids (or void clusters). Similarly, the cross-correlations between the grayscale values corresponding to "glass" and "void" represent the probability of the random vector landing with its tail in the glass phase and its head in the void phase. Hence the correlation map in this case indicates the average relative position of void with respect to the glass phase.

In order to calculate the two-point correlations, a function is defined in MATLAB that indicates the phase at each point of the samples: $m(\mathbf{x},h)$, where m takes the value 1 if phase h is present at point $\mathbf{x}$, or 0 otherwise. Then the two-point statistics for phases h and h' are defined formally by

$$f(h,h'|\mathbf{r}) = \frac{1}{vol(\Omega)}\int_{\Omega} m(\mathbf{x},h)m(\mathbf{x}+\mathbf{r},h')d\mathbf{x} \quad (1)$$

for any vector $\mathbf{r}$. Since this equation involves a convolution between the functions $m(\mathbf{x},h)$ and $m(\mathbf{x},h')$, these correlations can be computed very efficiently using fast Fourier transforms [37,38].

3. Results and Discussion

3.1. Constituent Properties

The 90° weft yarn in this fabric is relatively straight as it is not woven through the straight and stiff carbon tows in the 0° direction, as shown in Fig. 1(b). The undulating 0° warp yarns are woven through the weft yarns, creating obstacles for void escape in the interbundle gaps [19,20]. The architecture of this fabric causes a third class of voids, in addition to the customary interbundle and intrabundle voids, as shown in Fig. 2. These are termed "yarn voids" since they form at the yarns keeping the carbon fibre tows together. In summary, the three void types (Fig. 3) can be described as:

1. *Intrabundle voids*: small needle-shaped voids formed between individual filaments within the fibre bundles.
2. *Interbundle voids*: larger almost spherical voids, formed between bundles or close to bundle surfaces.
3. *Yarn voids*: the largest type of voids or void clusters following both the warp and weft yarns. They are generally long and may be curved or close to curved yarns.

The long, thin shape of the yarn voids is similar to the voids characterised in prepreg materials [31,32,34]. Examples of each are shown in 2-D slices of images from SRCT in Fig. 3. All types of voids can be regarded as defects, which have the potential to influence damage growth during loading. Generally larger voids or defects are often thought to be of higher concern [35], being possibly more likely to act as sites for damage formation [9]. Work by Scott et al indicates that fibre fracture is more prevalent

adjacent to voids in 0° plies under tensile loading [39]. This motivates a closer investigation of the yarn voids, how they form and their interaction with crack growth.

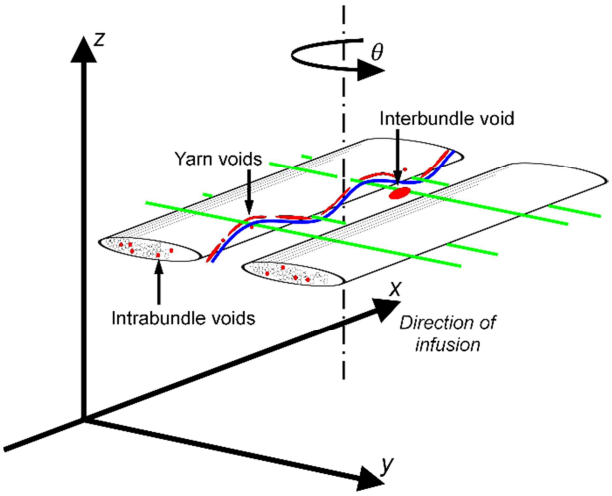

Fig. 2. Classification of identified voids.

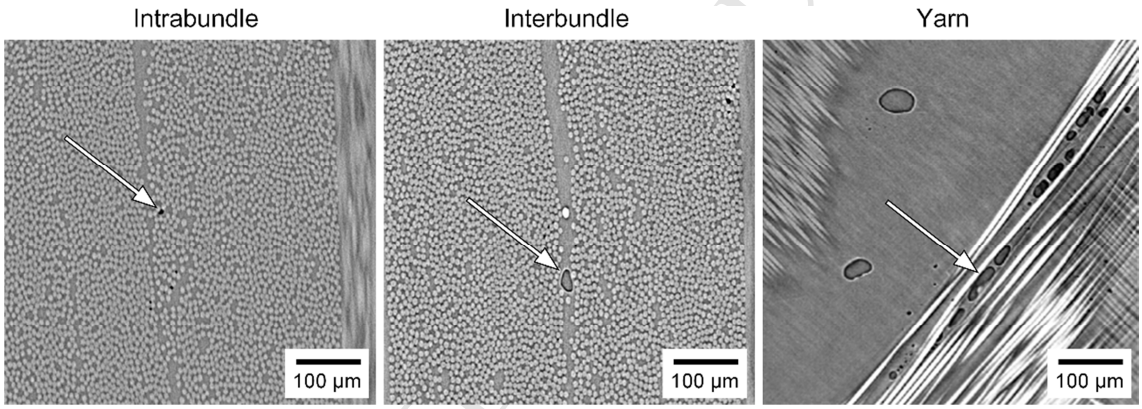

Fig. 3. SRCT 2D slice images of voids at three different locations.

An example 3-D image (5.86 × 4.21 × 4.13 mm^3) obtained by CT is shown in Fig. 4 with the carbon fibre and resin partially removed from the volume. The yarns of the different layers and the larger yarn voids highlighted in red are clearly visible. Void clustering is easily seen, where the voids appear to be arranged in planar layers (grouped at particular heights through the laminate thickness). The voids appear to be clustered along the fibre yarn bundles and sometimes also along the carbon fibre bundles.

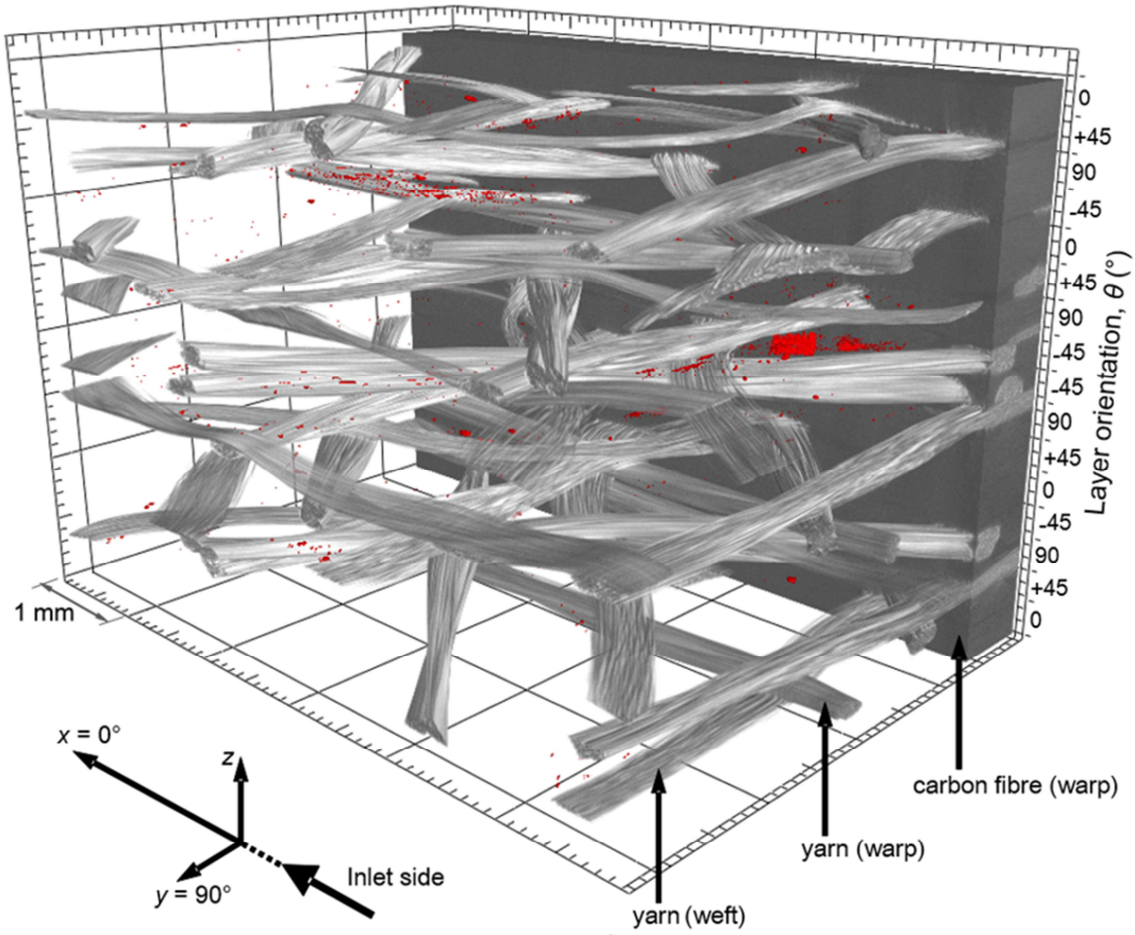

Fig. 4. A 3-D µCT rendering of the laminate showing yarn bundles and larger voids in 5.86×4.21×4.13 mm^3 volume.

3.2. Analysis of Void Distribution and Morphology

The surface of a contour of the void autocorrelation map is shown in Fig. 5. This contour map can be regarded as the average shape of the overall assembly of voids based on the probability that a given vector in the *x*-*y*-*z* space falls inside the void phase [37,38]. Fig.5a indicates that the void clusters extend primarily along the 0°, +45° and 90° directions, with significantly fewer voids orientated in the –45° direction. This agrees with the visual analysis of Fig. 4 that shows voids primarily clustering around and along the glass tows in the same directions. Fig. 5a emphasizes the in-plane nature of the void clusters, with very little spread in the through-thickness direction (Fig. 5b). The asymmetry of the orientation distribution in the +45° and –45° layers cannot be explained at the present stage, but it is noted that their neighbouring layers are not the same in the $[0/–45/90/+45]_{2s}$ layup and that neighbouring layers inevitably influence the void formation due to flow gradients.

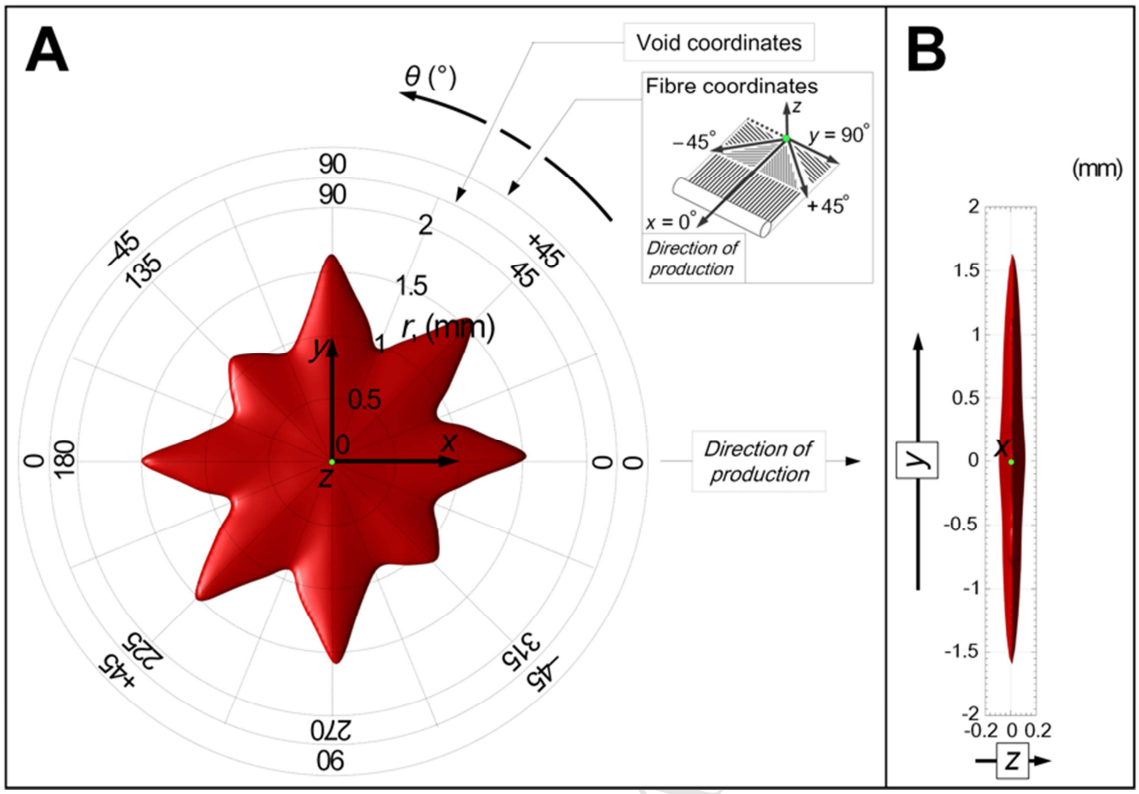

Fig. 5. Surface map of a single contour of the void autocorrelations for the µCT data, indicating the 'average' shape of voids / void clusters and the layer orientations.

The contour map in Fig. 5 indicates the shape of the void, but not the location. Analysis of the 3-D representation shows that very few voids were found in the 0° layers (fibres parallel to the resin flow direction) compared to the other layer orientations [13,16]. The observation of larger void formation in the off-axis layers can be explained by the voids trapped in those layers having difficulty escaping with the resin flow as compared to the direct inter-tow escape routes in layers where the fibre bundles are aligned with the flow [20]. The unidirectional carbon fibre tows, which comprise over 90% of the fibre reinforcement, act as obstacles for the voids when oriented transverse to the resin flow direction. The near absence of voids in the 0° layers supports this explanation. Any interbundle or yarn voids formed in the 0° layers have a high probability of escaping to the flow front in that same layer, or moving out-of-plane into an adjacent, off-axis layer and becoming entrapped there. Thus, the microstructural study focuses on the off-axis layers where a significant number voids are present, i.e. ±45° and 90°.

In order to quantify the dimensional and spatial distribution of voids, a small volume ($8 \times 4 \times 1.6$ mm^3) containing the middle six layers was chosen and quantitatively analysed with respect to the volume and location in the thickness direction using the SRCT image slices. Fig. 6 presents the distribution results for the void size and *z*-axis location, in relation to the approximate locations of the layer interfaces and the yarns intersecting the investigated volume. Locally, the thickness of each layer deviates from the average thickness (250 µm) because of layer heterogeneity and "nesting".

Fig. 6 illustrates the accumulation of voids along the layer interfaces and also relative to the yarns. The voids are concentrated at either the layer interfaces or along the yarns. The accumulation of interbundle voids along the fibre bundle surfaces has also been observed elsewhere, and those voids were reported to be generally more difficult to eliminate during processing than other interbundle voids [11]. This could be explained by the shear flow resistance exerted on bubbles adhering to fibre surfaces. The accumulation of voids along the yarn fibres is likely to be due to a similar mechanism, and this is enhanced by the increased tortuosity of the interbundle flow path due to the yarns.

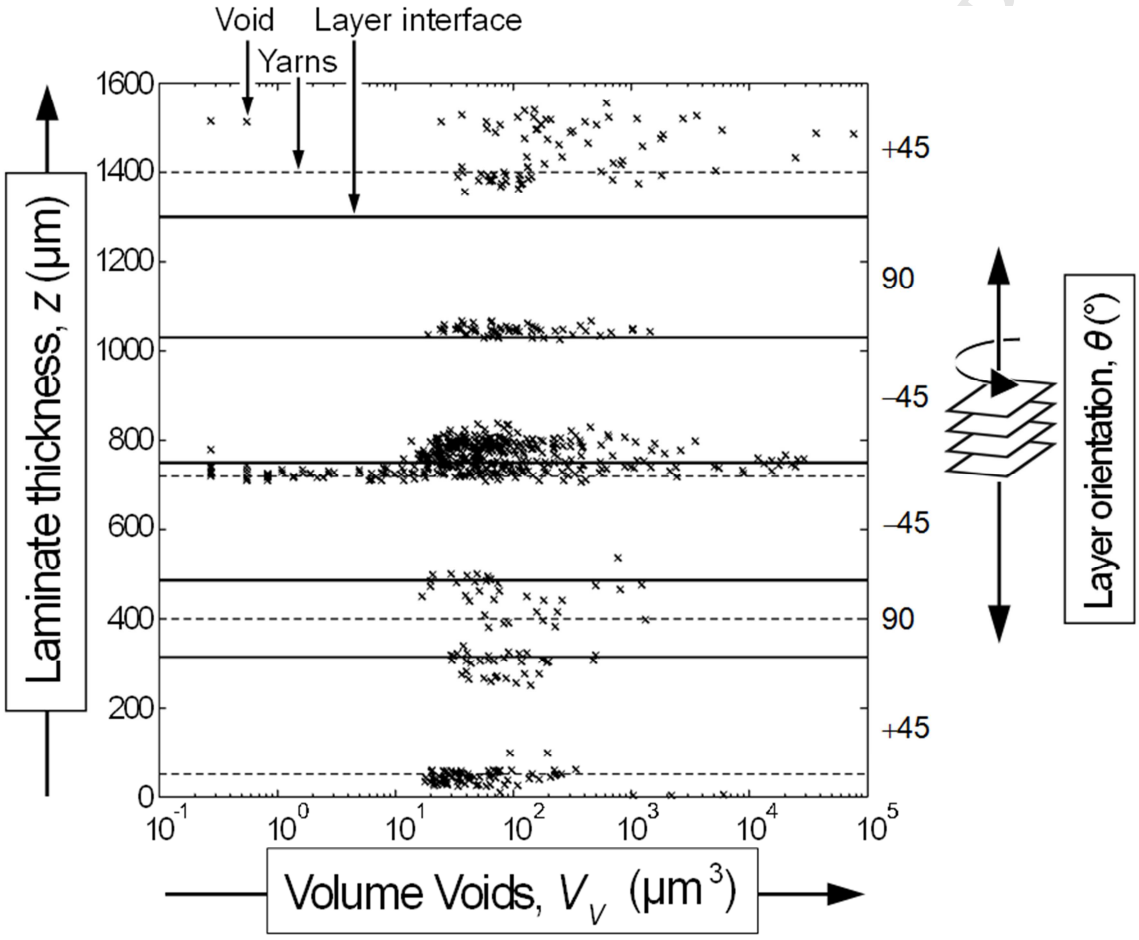

Fig. 6. SRCT image analysis of the spatial distribution of voids in terms of *z*-axis location and size for sample volume covering the off-axis middle six layers.

Flow in the gaps between layers also experiences shear resistance at the fabric surfaces where voids are likely to adhere, in a similar mechanism by which interbundle voids adhere to tows along the interbundle pathways [1,45,46]. Additionally, the difference in permeability of neighbouring layers results in an uneven flow front which can generate further voids.

The layer-to-layer interface area could be considered simply as a larger case of the interbundle gap than the interbundle gaps within a layer, but the larger size of the gaps must be accommodated. Models for void formation or subsequent void mobility must be adapted to the laminate-scale of the fabric (beyond simply fibres and bundles) to be accurate for industrial processing.

As also shown in Fig. 6, the size of the detectable individual voids in this volume exhibits a range of several orders of magnitude, from 10 to 1,000 µm^3. This distribution suggests a "bell-curve" number distribution of void sizes, i.e. the highest frequency of size is the median value, with decreasing frequency as the size increases or decreases from there. Such a distribution has been previously observed for interbundle gap widths and related to void sizes [9,17].

A subset of the image slices was analysed slice-by-slice along the width, in the *y*-direction to record the total volume of voids in each image slice, delineated by the layer in which the voids are located, as shown in Fig. 7. Delineation by layer can only be an approximation, because the interfacial location of the majority of voids makes it difficult to decide which side of the boundary each void belongs to. These image slices were oriented so that the planar images are parallel to both the *x*-axis (direction of flow) and the *z*-axis (laminate thickness). Thus the slice-by-slice analysis shows the void volume distribution along the *y*-axis, i.e. transverse to the flow direction. One can see a periodic distribution of void content in the ±45° layers; the -45° layers have peaks in void content every ~1200 µm and the +45° layers have single peaks near the middle of the 1500 µm width. The 90° layers show a more uniform void concentration across the analysed width.

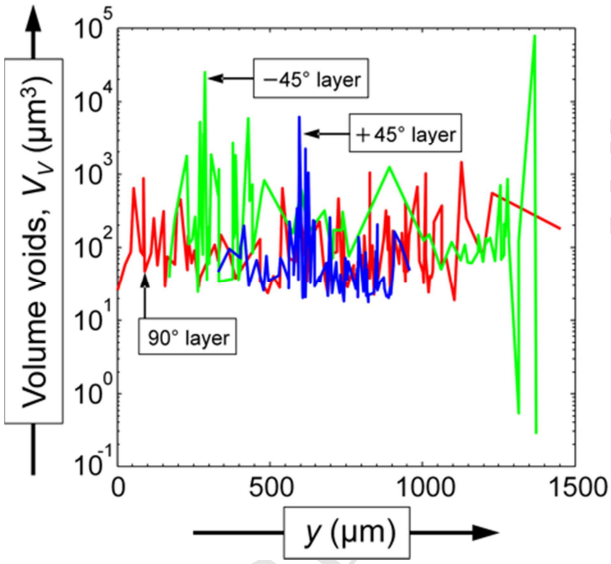

Fig. 7. SRCT image analysis showing the heterogeneous void distribution transverse to the infusion and thickness direction.

The void concentration in the transverse *y*-direction for ±45° layers is suspected to be caused by the yarn distribution. A periodicity of 1200 µm is consistent with the distances between yarn fibre bundles. Voids formed in non-crimp fabrics (NCFs) have been shown to move along and then be trapped by stitching fibres [5,9,13,17,40]. The glass yarns in the fabric used in this study are assumed to trap bubbles similar to stitching fibres in an NCF. The stitching fibres in NCFs have the same function as the yarns in the present fabric, namely to keep the reinforcing carbon fibre bundles in place. Flow of resin with voids has also shown an accumulation of voids at any obstruction along off-axis fibres [12,20]. Hence, the spacing of peaks in void concentration should be similar to the spacing between the yarns, as observed here.

The size and location of the voids is shown in Fig. 8 for each layer in each off-axis orientation (±45° and 90°) in the *x*-*y*-plane as observed from above the layers. The size of these voids is shown by colours, where the purple shades correspond to the largest and thought to be most severe. Diagonal and fairly linear clusters of voids are seen in all layer orientations. The diagonal orientation of the voids in the ±45° layers is likely to be due to the bias orientation of the carbon fibres and yarns. However, the diagonal orientation of the 90° layer is more difficult to explain. It suggests a strong out-of-plane effect on bubble formation and bubble flow; i.e. faster flow in the diagonal direction and diagonal clustering of the voids in the bias-direction layers both seep into the adjacent 90° layers due to the slower flow there. Voids may be formed in the 90° layers due to the difference in flow rates, and migrating bubbles from the adjacent layers immediately become entrapped by the transverse-to-flow fibres. Void formation and its patterns cannot be considered as independent factors in the various layers, but are intimately affected by these processes in the neighbouring plies.

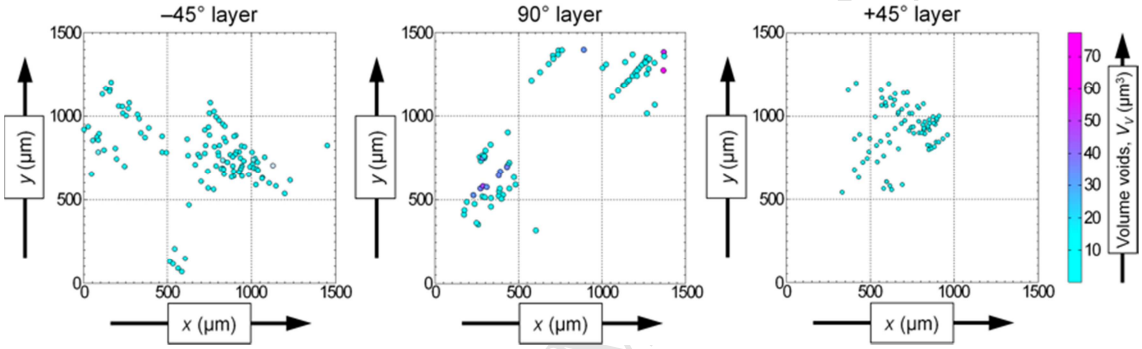

Fig. 8. SRCT image analysis showing in-plane void distribution in the –45°, 90° and +45° layers.

Out-of-plane flow has been presented as a mechanism for bubbles to avoid entrapment by obstacles [20]. Out-of-plane resin flow has also been modelled numerically [41], but to the authors' knowledge no experimental or analytical work has yet treated the out-of-plane flow's effect on void formation or migration. The typical model for interbundle and intrabundle void formation could be extended to laminate-scale void formation between adjacent fabric layers of different orientations. The flow in layers with fibres aligned with the flow, i.e. 0° layers, is nearly always faster than in off-axis layers due to the higher permeability caused by oriented interbundle gaps that promote flow channelling [42]. Thus the faster flow in the parallel fibres of 0° unidirectional layers can locally cause *z*-direction fluid seepage into the adjacent off-axis layers ahead of the flow front in those layers. This seepage into the adjacent layers, ahead of the flow front in that layer, would entrap air bubbles, leading to voids in the off-axis layers. This is similar to the same mechanism responsible for the void formation pattern due to differences in interbundle and intrabundle flow front positions [1], but considered now at the laminate scale, for different flow front positions in adjacent fabric layers. This seepage is likely to also cause a migration of bubbles formed in the 0° layers to the surrounding layers, especially due to encountering obstructions in the 0° layer such as the weft yarns. The same pattern is expected to occur due to seepage from the faster flow in ±45° layers to the slower flow in the 90° layers, transferring the 45° void arrays into the 90° layers (Fig. 8).

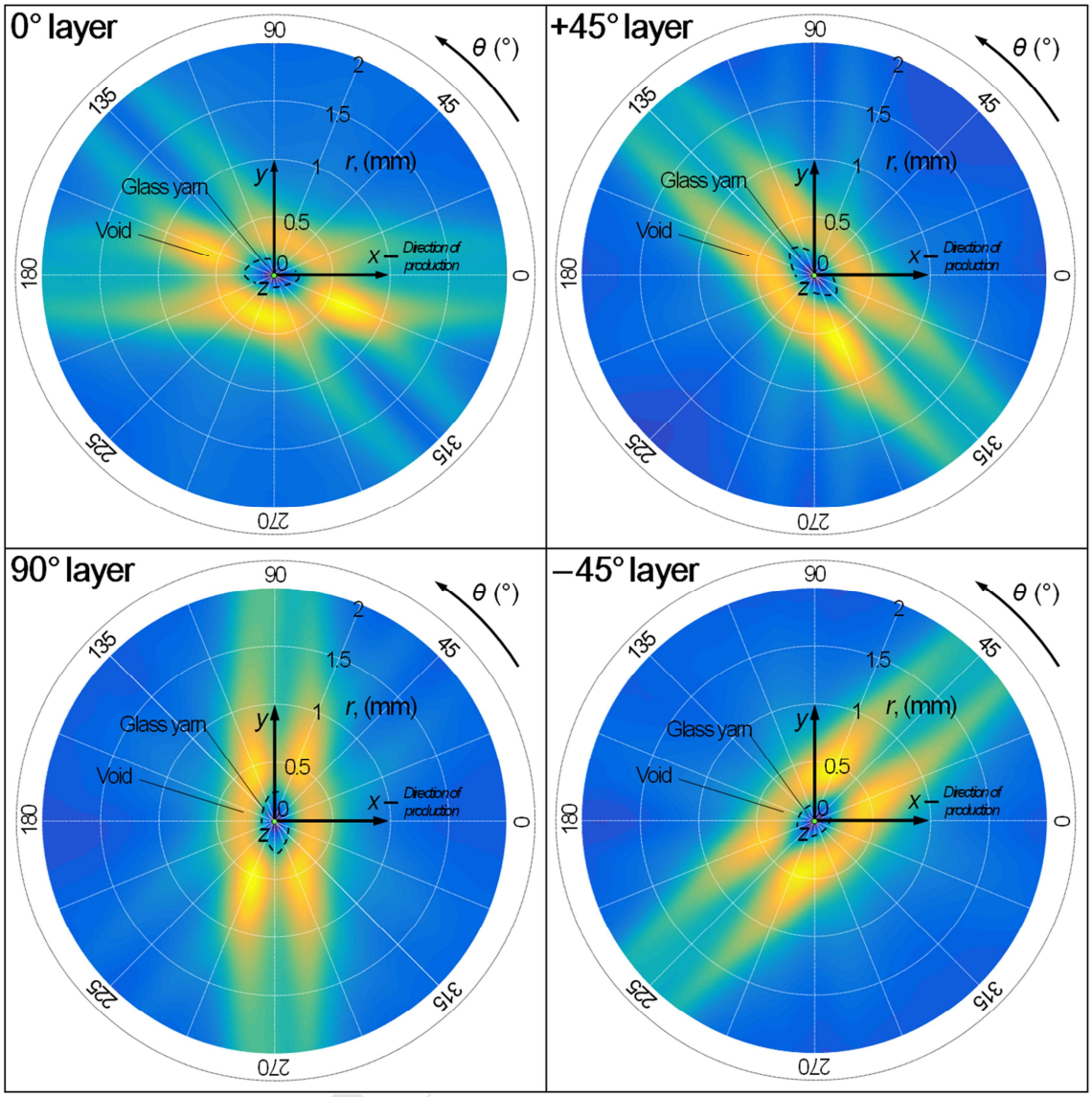

Fig. 9. In-plane glass-void cross correlation maps in the various sub-layers of the sample obtained from the µCT data. The yellow regions indicate areas with a high probability of void location relative to an average position in the glass (located at the center of the image).

Fig. 9 illustrates the two-point cross correlation between the glass and void phases in the sample for sublayers of different ply orientation. The position in the centre of each image may be thought of as an average point in the glass yarn. Then the colouring at a position relative to that point indicates the probability of finding a void region in that area relative to the glass yarn. The figure is a representation of the empirical probability of drawing a vector in the volume starting in the supporting yarn material and ending inside a void. While the 0° layer is clearly affected by the neighbouring 45° layer, the images generally tell a consistent story: the voids are located in the plane of the glass tows, with a fairly even distribution in front and behind the tow relative to the infusion direction. In each case there is a slightly higher probability of finding voids in front of the tow rather than behind it. Very few voids are found out-of-plane relative to the glass (although this cross section of the correlation map is not shown).

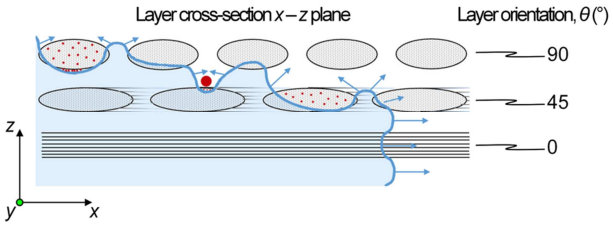

Fig. 10. Schematic of through-thickness resin flow (blue arrows) and predicted areas of void formation (red) in multi-axial reinforcement. Bulk flow in *x* direction.

Clustering of voids, similar to the schematic shown in Fig. 10, has been shown to have a significant effect on crack propagation during mechanical loading [25]. A dense cluster of smaller voids may have a similar effect on crack growth as a single large void of the same volume. Fig. 10 also shows that the individual voids are relatively small in the ±45° layers, whereas the larger voids are almost exclusively found in the 90° layer (Fig. 8) and can span dozens of fibres with a characteristic dimension greater than the fibre tow thickness [23,43,44]. Micrographs have shown the tendency for crack initiation and propagation from larger voids [9], which has been confirmed by a previous study on a different material using CT [10]. The larger voids in the 90° layers thus suggest those layers to be of the most concern in terms of affecting the mechanical performance.

3.3. Implications of findings

Process tuning for void minimisation can be supported by inter- and intra-bundle void formation modelling [45]. Further work to expand such models to out-of-plane flow and laminate-scale models of the fibre architecture including woven or stitched fibre architectures could improve these models. Minimisation of voids accumulated at the layer interfaces and at yarns could then suppress the formation of damage and premature failure of RTM composites based on UD weaves [4,9,39,47].

These studies demonstrated that the sensitivity of crack accumulation to voids also increases from a low value in the 0° layers, through the ±45° layers to a high value in the 90° layers [4-9]. Thus the problem of voids for this flow and test orientation is compounded by two important characteristics: (i) more and larger voids are formed in the layers transverse to the local flow, and (ii) while the 90° fibres do not contribute substantially to tensile strength in the 0° direction, voids in this direction are more likely to induce growth and general damage propagation under tensile loading [4-9]. These observations draw attention to the possibility of infusing a composite component in a direction that would minimise the effect of the resultant voids. Infusing a part in a direction transverse to the expected primary load direction would create the fewest voids in the transverse-to-load direction and thus minimise the effect of voids on fatigue strength. Most composite parts are loaded in multiaxial directions, thus complicating this strategy. Opportunities are evident, however, to optimise the mechanical performance based on flow direction and velocity. This is especially the case for long slender structures with predominantly unidirectional fibres. Guidelines in positioning inlets and outlets in resin infusion are otherwise mainly concerned with minimising the production cycle times and to eliminate dry spots [46]. For high-end composite applications, the mechanical performance could be more important than the production costs.

4. Conclusions

The observations in this study lead to three main conclusions regarding voids in RTM of a multi-axial lay-up of a fabric. First, the voids are much more likely to be located in the layers where the fibres are not parallel to the flow direction. The larger is the off-axis angle, the higher the void content and the larger the voids. Second, the voids are concentrated at the layer interfaces and along the yarns. Third, out-of-plane resin flow and bubble-flow appear to be a significant mechanism for void formation and void mobility as the distribution of small voids in the 90° layers follows the diagonal pattern of the adjacent bias-direction plies.

The tendency for void formation is higher in layers obliquely oriented to the infusion direction, and the associated risk with tensile damage formation in these off-axis layers has been shown to increase in the presence of these voids, whereas the 0° tensile strength is less affected by voids. Infusion perpendicular to the expected loading direction is recommended as it would generate more voids in the 0° layers and less voids in the more sensitive 90° layers.

Further research regarding the optimisation of infusion strategies with regard to structural performance such as fatigue resistance and damage tolerance while maintaining the cost benefits of using an out-of-autoclave process will be important for high-performance composite applications. The combined use of high resolution computed tomography, 3-D shape characterisation and statistics of the void microstructure in RTM produced material has been shown to be a powerful technique which is likely to be important in further exploring such processes.

Acknowledgements

We are grateful to the the µ-VIS centre at the University of Southampton for the provision of tomographic imaging facilities, supported by EPSRC grant EP-H01506X, and the Swiss Light Source (SLS) for access to the synchrotron beamline TOMCAT-X02DA, supported by SLS grant 20131256. We also acknowledge support from M.N. Mavrogordato, P. Modregger, I. Sinclair, G. Borstnar, S. Ahmed, D.J. Bull, P.A.S. Reed, E. Olsson, and F. Edgren. We are grateful for the materials that have been supplied by GKN Aerospace.

References

1. Patel N, Lee L. Effects of fiber mat architecture on void formation and removal in liquid composite molding. Polym Compos 1995;16:386–99.

2. Park C, Woo L. Modeling void formation and unsaturated flow in liquid composite molding processes: a survey and review. J Reinf Plast Compos 2011;30:957-77.

3. Tang JW, Lee, G. Springer. Effects of cure pressure on resin flow, voids, and mechanical properties. J Compos Mater 1987;21:421–40.

4. Almeida S, Neto Z. Effect of void content on the strength of composite laminates. Compos Struct, 1994;28:138-48.

5. Olivier P, Cottu J, Ferret B. Effects of cure cycle pressure and voids on some mechanical properties of carbon/epoxy laminates. Composites 1995;26:509-15.

6. Huang H, Talreja R. Effects of void geometry on elastic properties of unidirectional fiber reinforced composites. Compos Sci Tech 2005;65:1964-81.

7. Guo Z, Liu L, Zhang B, Du S. Critical Void Content for Thermoset Composite Laminates. J Compos Mater 2009;43:1775-90.

8. Varna J, Joffe R, Berglund L, Lundström TS. Effect of Voids on Failure Mechanisms in RTM Laminates. Compos Sci Tech 1995;53:241-49.

9. Sisodia S, Gamstedt EK, Edgren F, Varna J. Effects of voids on quasi-static and tension fatigue behaviour of carbon-fibre composite laminates. J Compos Mater 2015;49:2137-48.

10. Lambert J, Chambers A, Sinclair I, Spearing SM. 3D damage characterisation and the role of voids in the fatigue of wind turbine blade materials. Compos Sci Tech 2012:72-337-43.

11. Hamidi Y, Aktas L, Altan M. Effect of packing on void morphology in resin transfer molded E-Glass/epoxy composites. Polym Compos 2005;26:614-27.

12. Rohatgi V, Patel N, Lee L. Experimental investigation of flow- induced microvoids during impregnation of unidirectional stitched fiberglass mat. Polymer Compos1996:17:161-70.

13. Lundström TS, Gebart BR. Influence from process parameters on void formation in RTM. Polymer Compos1994;15:25-33.

14. Gourichon B, Binetruy C, Krawczak P. A new numerical procedure to predict dynamic void content in liquid composite molding. Composites Part A 2006;37:1961-9.

15. Lundström. TS. Measurement of void collapse during transfer moulding. Composites Part A 1997;28A:201-14.

16. Matsuzaki R, Seto D, Todoroki A, Mizutani Y. Void formation in geometry–anisotropic woven fabrics in resin transfer molding. Adv Compos Mater 2014;23:99-114.

17. Frishfelds V, Lundström TS, Jakovics A. Bubble motion through non-crimp fabrics during composites manufacturing. Composites Part A 2008;39:243-51.

18. Shih C, Lee L. Analysis of void removal in liquid composite molding using microflow models. Polym Compos 2002;23:120–31.

19. Kang K, Koelling K. Void transport in resin transfer molding. Polym Compos 2004;25:417–432.

20. Lundström TS, Frishfelds V, Jakovics A. Bubble formation and motion in non-crimp fabrics with perturbed bundle geometry. Composites Part A 2010;41:83-92.

21. Park C, Lebel A, Saouab A, Breard J, Lee, W. Modeling and simulation of voids and saturation in liquid composite molding processes. Composites Part A 2011;42:658–68.

22. Gueroult S, Bizet L, Breard J. Experimental determination of void formation and transport in the RTM process. Proc. FPCM 11, 2012.

23. Vilà J, Sket F, Wilde F, Requena G, González C, Llorca J. An in situ investigation of microscopic infusion and void transport during vacuum-assisted infiltration by means of X-ray computed tomography. Compos Sci Tech 2015;119:12-19.

24. Jinlian H, Yi L, Xueming S. “Study on void formation in multi-layer woven fabrics.” Composites Part A 2004;35:595–603.

25. Fullwood DT, Gerrard DD, George AR, Halverson DM. Dispersion metrics for composites – a machine learning based analysis. Proc. SAMPE International Conference, 2013:1-12.

26. ASTM Standard D3171, 2011, Standard test methods for constituent content of composite materials. DOI: 10.1520/D3171-11.

27. George AR, Dart R, Brandley M, Zsiros J. Quick Measurements of Void Content in Fiberglass Reinforced Composite Materials. Proc. 45th ISTC, 2013.

28. Liu L, Zhang B, Wang D, Wu Z. Effects of cure cycles on void content and mechanical properties of composite laminates. Compos Struct 2006;73:303-9.

29. George A, Brandley M, Dart R, Fullwood DT. Void Modeling in Resin Infusion. J Adv Mater 2015;1:79-93.

30. Centea T, Hubert P. Measuring the impregnation of an out-of-autoclave prepreg by micro-CT. Compos Sci Tech 2011;71:593-9.

31. Hernandez S, Sket F, Molina-Aldareguıa J, Gonzalez C, LLorca J. Effect of curing cycle on void distribution and interlaminar shear strength in polymer-matrix composites. Compos Sci Tech 2011;71:1331-41.

32. Zhang D, Heider D, Advani SG, Gillespie JW. Out of Autoclave Consolidation of Voids in Continuous Fiber Reinforced Thermoplastic Composites. Proc. SAMPE International Conference, 2013:1-16.

33. Nikishkov Y, Airoldi L, Makeev A. Measurements of voids in composites by X-ray Computed Tomography, Compos Sci Tech 2013;89:89-97.

34. Hernández S, Sket F, González C, LLorca J. Optimization of curing cycle in carbon fiber-reinforced laminates: void distribution and mechanical properties. Compos Sci Tech 2013;85:73-82.

35. Schell J, Deleglise M, Binetruy C, Krawczak P, Ermanni P. Numerical prediction and experimental characterisation of meso-scale-voids in liquid composite moulding. Composites Part A, 2007;38:2460-70.

36. Dowd BA, Campbell GH, Marr RB, Nagarkar V, Tipnis S, Axe L, Siddons DP. Developments in synchrotron x-ray computed tomography at the National Synchrotron Light Source. Proc. SPIE 3372, 1999.

37. Fullwood DT, Niezgoda SR, Kalidindi SR, Adams BL. Microstructure sensitive design for performance optimization, Prog Mat Science, 2010;55:477-562.

38. Torquato S. Random Heterogeneous Materials. Springer-Verlag, 2002.

39. Scott AE, Sinclair I, Spearing SM, Mavrogordato MN, Hepples W. Influence of voids on damage mechanisms in carbon/epoxy composites determined via high resolution computed tomography. Compos Sci Tech 2014;90:147-153.

40. Aranda S, Klunker F, Gabber H, Ziegmann G. Void content and void formation mechanisms in resin infusion processes. Proc. SEICO, 2009.

41. Calado V, Advani S. Effective average permeability of multi-layer preforms in resin transfer molding. Compos Sci Tech, 1996;56:519-31.

42. Gebart BR. Permeability of unidirectional reinforcements for RTM. J Compos Mater 1992;26:1100-33.

43. Verrey J, Michaud V, Manson J. Dynamic capillary effects in liquid composite moulding with non-crimp fabrics. Compos Part A 2006;37:92-102.

44. Li M, Wang S, Gu Y, Zhang Z, Li Y, Potter K. Dynamic capillary impact on longitudinal micro-flow in vacuum assisted impregnation and the unsaturated permeability of inner fiber tows. Compos Sci Tech 2010;70:1628-1636.

45. Ruiz E, Achim V, Soukane S, Trochu F, Breard J. Optimization of injection flow rate to minimize micro/macro-voids formation in resin transfer molded composites. Compos Sci Tech 2006;66:475-86.

46. Advani SG, Bruschke MV, Parnas R. Resin transfer molding. In: Flow and rheology in polymeric composites manufacturing Amsterdam: Elsevier; 1994:465-516.

47. Munoz R, Gonzalez C, Llorca J. Mechanisms of in-plane shear deformation in hybrid three-dimensional woven composites. J Compos Mat 2016;30:3755-63.